

Overlap Distribution of the Three-Dimensional Ising Model

Bernd A. Berg^{1,2}, Alain Billoire² and Wolfgang Janke³

(E-mail: berg@hep.fsu.edu, billoir@sphs.saclay.cea.fr, wolfgang.janke@itp.uni-leipzig.de)

¹Department of Physics, The Florida State University, Tallahassee, FL 32306, USA²CEA/Saclay, Service de Physique Theorique, 91191 Gif-sur-Yvette, France³Institut für Theoretische Physik, Universität Leipzig, 04109 Leipzig, Germany
(May 15, 2002)

We study the Parisi overlap probability density $P_L(q)$ for the three-dimensional Ising ferromagnet by means of Monte Carlo (MC) simulations. At the critical point $P_L(q)$ is peaked around $q = 0$ in contrast with the double peaked magnetic probability density. We give particular attention to the tails of the overlap distribution at the critical point, which we control over up to 500 orders of magnitude by using the multi-overlap MC algorithm. Below the critical temperature interface tension estimates from the overlap probability density are given and their approach to the infinite volume limit appears to be smoother than for estimates from the magnetization.

PACS: 05.50.+q Lattice theory and statistics (Ising, Potts, etc.), 75.40.Mg Numerical simulation studies, 75.10.Hk Classical spin models, 75.10.Nr Spin-glass and other random models.

I. INTRODUCTION

In this paper we investigate the two replica overlap probability density $P_L(q)$ for the three-dimensional (3d) Ising model. On a L^3 lattice with periodic boundary conditions q is defined by

$$q = \frac{1}{N} \sum_{i=1}^N s_i^{(1)} s_i^{(2)} \quad \text{with } N = L^3; \quad (1)$$

where $s_i^{(1)}$ and $s_i^{(2)}$ are the spins of two copies (replica) of the system at temperature $T = 1$. The distribution of the overlap q is of major importance in spin-glass investigations [1,4], where it plays the role of an order parameter, often called Parisi order parameter.

To our knowledge this quantity has never been investigated for simple spin systems like the 3d Ising model. One reason is certainly that one has in that situation the magnetization m as an explicit order parameter at hand and a description of the critical properties based on the magnetic probability density $P_L^m(m)$ is believed to be identical to one based on $P_L(q)$, in particular $h q_i = h m_i^2$. However, the overlap probability density is an interesting object for study on its own merits and we find remarkable differences between the shapes of $P_L(q)$ and $P_L^m(m)$. Therefore, we find it worthwhile to have the properties of $P_L(q)$ documented for the Ising model, which is by orders of magnitude easier to simulate than spin glasses, since the dynamics is much faster and only one (instead of many) realization needs to be simulated.

In the vicinity of the critical point, by finite-size scaling (FSS) arguments [5] $P_L(q)$ can, in leading order for L large, be written as

$$P_L(q) = \frac{1}{L} P^0(q^0) \quad \text{with } q^0 = \frac{q}{L}; \quad (2)$$

Here P^0 is a universal, L -independent function and L is the standard deviation of q with respect to the prob-

ability density $P_L(q \in [-1; +1])$ (or $P_L(q \in [0; 1])$ when appropriate).

A major focus of our investigation is on the tails of the $P_L(q)$ distribution, which we control for $L = 36$ at T_c over 500 orders of magnitude by using the multi-overlap MC algorithm [6]. This is also of interest in view of a conjecture by Bramwell et al. [7,8] that a variant of extreme order statistics describes the asymptotics of certain probability densities for a large class of correlated systems. Besides the Ising model with some $T(L) \rightarrow T_c$ as $L \rightarrow \infty$, their class includes the 2d XY model in the low temperature phase, turbulent flow problems, percolation models and some self-organized critical phenomena. For large L the asymptotic behavior is claimed to be described by an L -independent curve, which for the overlap variable would read ($q^0 \rightarrow 1$)

$$P^0(q^0) = C \exp \left[-a \frac{q^0 - q_{\max}^0}{q_{\max}^0} \right] e^{b(q^0 - q_{\max}^0)^i}; \quad (3)$$

Here C, a, b are constants and $q_{\max}^0 = q_{\max}/L$, where q_{\max} is the position of the maximum of the probability density $P_L(q)$ at positive q . Equation (3) is a variant of Gumbel's first asymptote [9], see [10,11] for reviews of extreme order statistics.

However, Eq. (3) is in contradiction with the widely accepted large-deviation behavior, based on the proportionality of the entropy with the volume [12],

$$P_L(q) \sim \exp[-N f(q)]; \quad (4)$$

where, for large N , $f(q)$ does not depend on N . Our data support Eq. (4). Using the ultimate magnetical approach [13] a similar study of the tails could be performed for the magnetic probability density $P_L^m(m)$, but this is outside the scope of our present paper.

We like to point out that for the overlap distribution of spin glasses the status of Eq. (4) is unclear due to the quenched average. Our previously reported result [14] demonstrates that for the 3d Edwards-Anderson Ising

spin glass a probability distribution of the form (3) gives an excellent description of the tails of the Parisi overlap distribution. Because of the special nature of its phase transition, Eq. (4) may also be questioned for the 2d X Y model, where the extreme order asymptotics (3) (more precisely a variant of it) with $a = -2$ is found in the spin wave approximation [7,8]. However, the range of validity of this perturbative argument is unclear, at least to us. It may be worthwhile to employ the methods of Ref. [13], or those of the present paper, to perform a careful numerical investigation of the 2d X Y model with respect to these questions.

We have performed simulations at and below the critical (Curie) temperature T_c of the Ising model phase transition. We approximate T_c by the value of Ref. [15]

$$c = \frac{1}{T_c} = 0.221\,654 \quad (5)$$

and present our results for T_c in Sect. II. Besides addressing the question of the asymptotic behavior of the overlap distribution, we estimate the critical exponent ratio $2 =$ from the FSS behavior of the standard deviation σ_L . For the temperatures below the Curie temperature we choose

$$\beta_1 = 0.232 \text{ and } \beta_2 = 0.3 : \quad (6)$$

For $\beta = 0.232$ multimagnetical results are available [16], which determine the probability density $P_L^m(m)$ of the magnetization over many orders of magnitude.

Our numerical results were obtained with the spin-glass code of the investigations of [6,14,17] by simply choosing all the exchange coupling constants to be equal to +1. A code which is specialized to the Ising model would be far more efficient. Therefore, we have limited our present simulations to small and medium sized lattices. As the results appear already quite clear, there seems to be no particularly strong reason to push on towards (much) larger systems.

II. RESULTS AT THE CRITICAL TEMPERATURE

Figure 1 shows our overlap probability density results $P_L(q)$ at the critical temperature (5). They rely on a statistics of 32 independent runs (with different pseudo random number sequences) for lattices up to size $L = 30$ and on 16 independent runs for our largest lattice, $L = 36$. After calculating the multi-overlap parameters [6] the following numbers of sweeps were performed per repetition (i.e. independent run): 2^{19} for $L = 4$, 2^{21} for $L = 6$, 2^{22} for $L = 8$, 2^{23} for $L = 12$; 16 , 2^{24} for $L = 24$, 2^{25} for $L = 30$ and, again, 2^{24} for $L = 36$ (with the present computer program this lattice size became too time consuming to scale its CPU time properly). Not to overload Fig. 1 error bars are only shown for selected values of q , whereas the lines are drawn from all data. The probability densities are normalized to

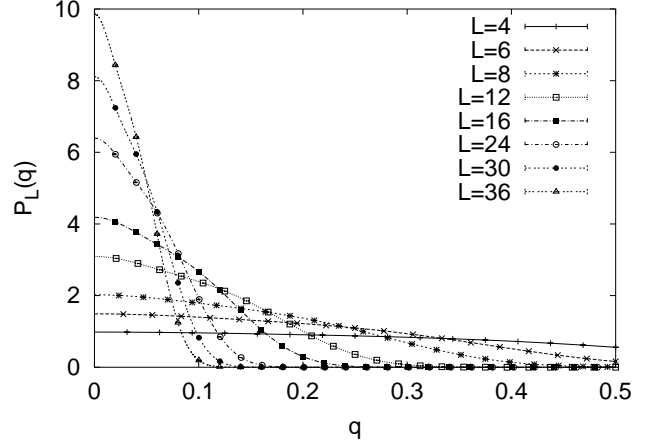


FIG. 1. Overlap probability densities at the critical point $c = 1/T_c = 0.221\,654$.

$$\int_{-1}^{+1} dq P_L(q) = 1 ; \quad (7)$$

and we show only the $q \geq 0$ part because of the symmetry $P_L(-q) = P_L(q)$. We cut the range at $q = 0.5$, because for $L \geq 8$ the probability densities are almost zero for $q > 0.5$.

Somewhat surprisingly we find the maximum of our $P_L(q)$ probabilities at $q_{\max} = 0$, in contrast to the magnetization where one finds a double peak at T_c , see for instance numerical data in Ref. [18] and analytical results of Ref. [19], both with periodic boundary conditions. In our simulation we kept a time series for the magnetization, which reproduces the expected double peaked histograms at T_c (as the accuracy of our magnetization histogram is lower than that of results in the literature, we abstain from giving a figure). Such differences are expected. For instance, while the two low-temperature magnetization values $m = \pm 1$ correspond to four overlap configurations, two with $q = +1$ and two with $q = -1$, the inverse is not true. There are altogether 2^N overlap configurations with $q = +1$ and another 2^N with $q = -1$.

Figure 2 shows $\ln[P_L(q)]$ versus q . The ordinate is cut off at 1000, to cover a range with results from at least two lattice sizes. The $L = 36$ lattice continues to exhibit accurate results down to 1200, thus the data from this system cover $1200 = \ln(10) = 521$ orders of magnitude.

The collapse of the $P_L(q)$ functions (2) on one universal curve $P^0(q^0)$ is depicted in Fig. 3. The figure shows some scaling violations, which become rather small from $L = 24$ onwards. The standard deviation σ_L behaves with L according to

$$\sigma_L / L^{1/2} = 1 + c_2 L^{-1} + \dots \quad (8)$$

Note that the ratio $\sigma_L / L^{1/2}$ is defined for the magnetization, and by FSS theory [5] $\sigma_L^m / L^{1/2} =$ holds for the

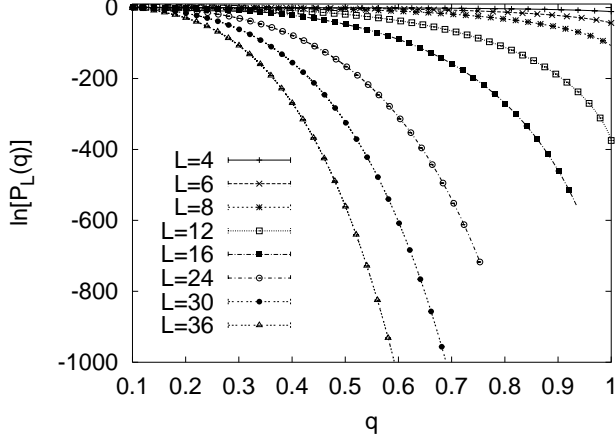


FIG. 2. Logarithm of the overlap probability densities at $c_c = 1/T_c = 0.221\,654$.

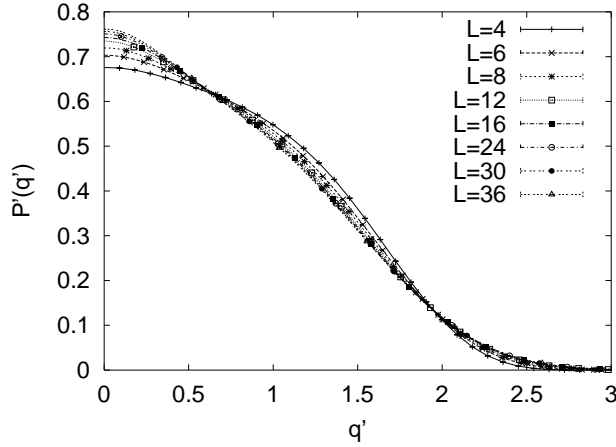


FIG. 3. Rescaled overlap probability densities $P^0(q^0) = L P_L(q)$ versus $q^0 = q - q_c$ at the critical point.

standard deviation of the magnetization. The factor of two difference in the exponent of Eq. (8) comes from dimensionality. Scaling relations and estimates of the Ising model critical exponents are reviewed in Ref. [20]. In particular, $2 = d/2 + \nu$ holds. Our estimate of $2 = \nu$ from a four-parameter fit of Eq. (8) to our data for the standard deviation σ_L is $2 = \nu = 1.0293(28)$ with $Q = 0.31$ the goodness of fit (see [21] for the definition of Q). Restricted to our $L \leq 24$ lattices the more stable two-parameter fit to the leading behavior of Eq. (8) gives

$$\frac{2}{\nu} = 1.030 \pm 0.005 \text{ with } Q = 0.36 : \quad (9)$$

The most accurate estimates of the literature [20] cluster around $\nu = 0.36$ with an error of a few units in the last digit. Within the conventional statistical un-

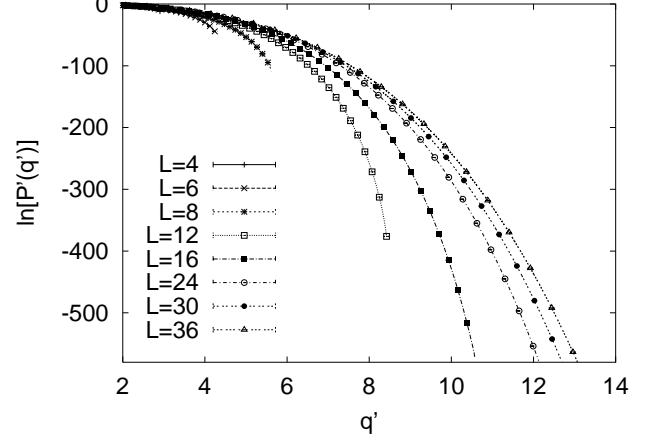


FIG. 4. Logarithm of the rescaled overlap probability densities $P^0(q^0) = L P_L(q)$ versus $q^0 = q - q_c$ at the critical point.

certainties this is consistent with our $2 = \nu$ values. The two-parameter fit becomes quickly inconsistent when the smaller lattices with $L < 24$ are included, with a trend towards smaller values of $2 = \nu$. Therefore, we conjecture that there will be a slightly increasing trend when larger lattices should become available. Because its larger error bar reflects to some extent systematic uncertainties, we prefer Eq. (9) over the four-parameter fit as our final estimate.

TABLE I. Deviation points for $4 \leq L \leq 36$ $|\ln[P_L^0(q^0)] - \ln[P_{36}^0(q^0)]| = 0.5$ of the $L = 4$ to 30 lattices from the $L = 36$ result.

L	4	6	8	12	16	24	30
q^0	2.27	2.46	2.65	2.95	3.25	3.83	4.54
q	0.781	0.580	0.472	0.351	0.288	0.225	0.212

In Fig. 4 we show the logarithm $\ln[P^0(q^0)]$ of the rescaled overlap probability densities and we see a breakdown of scaling for sufficiently large q^0 . The ordering of the lattices is that the rightmost curve corresponds to the $L = 36$ lattice. The smaller lattices deviate from it. From the left: First, the $L = 4$ lattice (not visible), next the $L = 6$, then $L = 8$, $L = 12$, $L = 16$, $L = 24$ and last $L = 30$. The agreement is over a larger and larger range in q^0 . However, scaled back to q , it concerns the vicinity of $q = 0$. To quantify this, we have collected in Table I the q^0 and corresponding q values at which the deviation

$$4 \leq L \leq 36 |\ln[P_L^0(q^0)] - \ln[P_{36}^0(q^0)]| = \ln[P_L^0(q^0)]$$

becomes $1/2$, a deviation too small to be visible on the scale of Fig. 4. The q^0 values are seen to increase, whereas the corresponding q values decrease.

It is well known that the requirement of consistency of a universal probability density (2) with the functional

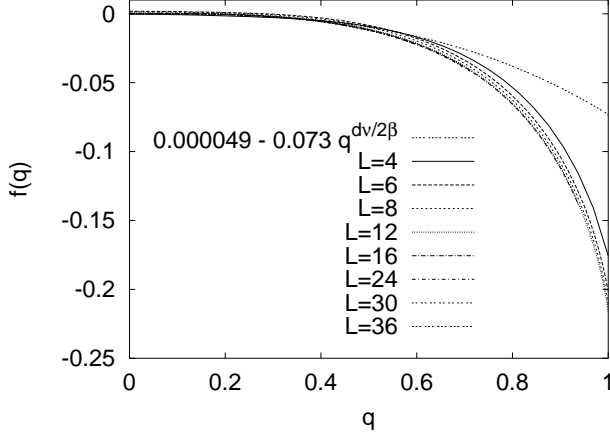


FIG. 5. The functions $f_L(q)$, extracted from Eq. (4) for various lattice sizes, are plotted together with a fit according to Eq. (11).

form (4) determines the function $f(q)$. Namely, to leading order the scaling of the function $(2) P_L^0(q^0)$ implies that

$$L^d f(q^0 L^{-2}) = g(q^0) \quad (10)$$

is an L -independent function. Therefore,

$$f(q) / q^{d/2} = \quad (11)$$

holds. Note that the non-critical Gaussian behavior is a special case, obtained for $d = 2$.

In contrast to Eqs. (2) and (11), the functional form (4) is expected to hold for all q , when L becomes large. This is easily tested by plotting

$$f_L(q) = \frac{1}{N} \ln [P_L(q)]; \quad (12)$$

as is done in Fig. 5, and seeing if $f_L(q)$ is L -independent up to $O(1/N)$ terms as it should. Not to obscure the behavior by too large symbols, the lines are plotted without error bars. A fit of the scaling form (11) to our $f_{36}(q)$ data for $q < 0.2$, $f(q) = 0.000049 - 0.073 q^{d/2}$ with $d = 1.030$ from Eq. (9), is also included in the figure.

We see excellent convergence towards an L -independent function, where the higher lying curves correspond to the smaller lattices ($L = 4$ being the one on top). However, the scaling behavior (11) only holds in the vicinity of $q = 0$. To make this quantitatively more precise, we subtract the function $f_{36}(q)$ from the others and plot the difference in Fig. 6 (at selected values of q we now include barely visible error bars by plotting $f_L(q) - f_{36}(q)$). In the large volume limit (for both of two lattices) the difference $[f_{L_1}(q) - f_{L_2}(q)]$ should be bounded by a constant

$$\left| \frac{1}{N_1} - \frac{1}{N_2} \right| :$$

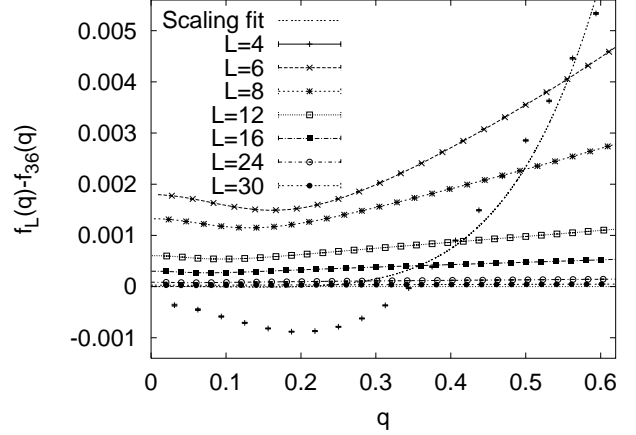


FIG. 6. The functions $f_L(q)$, as well as the fit to Eq. (11), with $f_{36}(q)$ subtracted (error bars are indicated at selected values of q).

We see in Fig. 6 that the $L = 24$ and 30 curves fall almost on the $L = 36$ one (the zero line). Note that the figure is cut off at $q = 0.62$. The number of sweeps needed to propagate the system over the full accessible q -range scales in the multi-overlap ensemble at least proportional to the system size N . Aiming at a comparable statistics for all system sizes, the required computer time thus grows at least proportional to N^2 . Therefore and because of numerical problems with the scaling point representation caused by the extreme smallness of $P_L(q)$ for $q \rightarrow 1$ when L is large, we restricted the overlap simulations to $q \in [0.7; +0.7]$ for the lattice sizes $L = 16, 24$, and 30 , and to $q \in [0.62; +0.62]$ for the $L = 36$ lattice. Nevertheless the smallest values of $P_L(q)$ we sampled were those of the $L = 36$ lattice.

On the basis of Eq. (4) the plots of Figs. 5 and 6 had to be expected. The conjecture (3) of Bramwell et al. [7,8] appears to be ruled out for the Ising model. Namely, when Eq. (3) (with $q_{max}^0 = 0$) and Eq. (12) are both valid in some region of $bq^0 = bL^2$, one ends to leading order

$$bqL^2 = d \ln(L) + \ln[f(q)]; \quad (13)$$

and $f(q)$ can only be L -independent if b is not a constant, but depends on q and L .

III. RESULTS BELOW THE CRITICAL TEMPERATURE

Below the critical temperature we made 16 independent runs per lattice size with the following numbers of sweeps per repetition: 2^{16} for $L = 4$, 2^{17} for $L = 6$, 2^{18} for $L = 8$, 2^{19} for $L = 12$, 2^{20} for $L = 16$ ($\beta = 0.232$) and 2^{21} for $L = 16$ ($\beta = 0.3$). The overlap probability

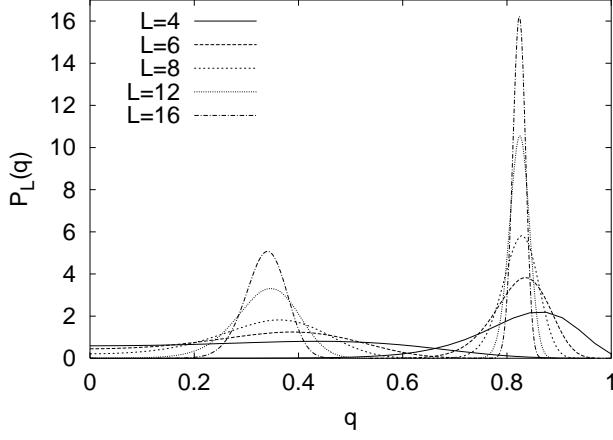


FIG. 7. Overlap probability densities at $\beta = 0.232$ (left set of curves) and $\beta = 0.3$ (right set of curves).

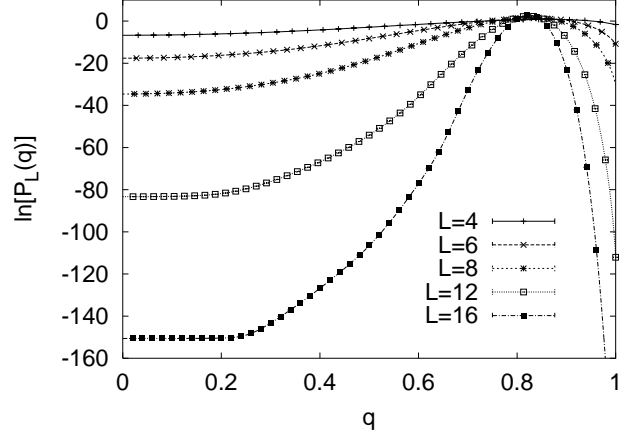


FIG. 9. Logarithms of the overlap probability densities at $\beta = 0.3$.

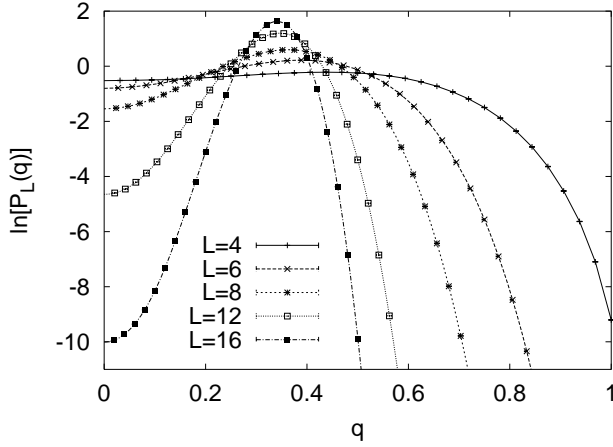


FIG. 8. Logarithms of the overlap probability densities at $\beta = 0.232$.

densities $P_L(q)$ for $\beta = 0.232$ and $\beta = 0.3$ are shown together in Fig. 7. Clearly, the peaks moved away from zero and are now at $q_{\text{max}} = 0.3408$ ($L = 16$; $\beta = 0.232$) and $q_{\text{max}} = 0.8237$ ($L = 16$; $\beta = 0.3$). In Figs. 8 and 9 we show the logarithms of these probability densities at $\beta = 0.232$ and $\beta = 0.3$, respectively. The scales in these two figures are chosen to accommodate all the $P_L(0)$ data, but not their tails, which continue down to much lower values. For the largest ($L = 16$) difference between $P_L(0)$ and the maximum of $P_L(q)$, we see that it increases from about four orders of magnitude at $\beta = 0.232$ to about 65 orders of magnitude at $\beta = 0.3$.

Note that the most likely $P_L(0)$ configurations are those where one replica stays around magnetization $m = 0$ and the other around the maximum of the magnetic probability density at positive or negative magnetization

TABLE II. Effective interface tension (16) results, $F_{s;L}$, from the overlap parameter at $\beta = 0.232$ and $\beta = 0.3$. At $\beta = 0.232$ results for the same quantity obtained in Ref. [16] from the magnetization density are included for comparison.

L	$\beta = 0.232$	$\beta = 0.232$ Ref. [16]	$\beta = 0.3$
4	0.00962 (27)	0.05297 (29)	0.23490 (33)
6	0.01416 (12)	0.03403 (15)	0.26325 (20)
8	0.016740 (82)	0.02779 (13)	0.28457 (20)
12	0.020281 (64)	0.02485 (12)	0.29751 (17)
16	0.022715 (34)	0.02521 (11)	0.29959 (11)

m . It follows that the ratio

$$R_L = \frac{P_L(0)}{P_L(q_{\text{max}})}; \quad (14)$$

where $P_L(q_{\text{max}})$ is the maximum of $P_L(q)$, is related to the interface tension F_s according to the formula introduced in [18] for the ratio $P_L^m(0) = P_L^m(q_{\text{max}})$,

$$R_L = C L^p \exp(-2L^2 F_s + \dots); \quad (15)$$

Here C, p are constants and $p = 1/2$ in the one-loop capillary wave approximation [22] or one-loop ϕ^4 -theory [19,23,24], compare the discussion in Ref. [25]. Two-loop ϕ^4 -theory is considered in Ref. [26]. The correction is large and it appears that a reliable estimate of p does not exist.

To determine the interface tension one may first calculate the lattice size dependent effective interface tensions

$$F_{s;L} = \frac{1}{2L^2} \ln R_L; \quad (16)$$

and then make an extrapolation of $F_{s;L}$ for $L \rightarrow \infty$. Table II collects our $F_{s;L}$ results where the error bars

with respect to the last digits are given in parentheses. For the sake of easy comparison, we list also some $F_{s;L}$ results of Ref. [16] at $\beta = 0.232$, obtained by applying the definitions (14) and (16) to the probability density of the magnetization. It is notable that the $F_{s;L}$ estimates from the overlap densities increase monotonically in the listed range of lattice sizes, whereas the $F_{s;L}$ estimates from the magnetization show a more complex behavior: Up to $L = 12$ they decrease, then they turn around to increase and the increase has been followed [16] up to lattices of size $L = 32$.

We pursue a similar fitting strategy as in Ref. [16]. As there, it turns out that our data do not really support fits to more than two parameters and that including the capillary wave term with the one-loop theoretical coefficient p does not lead to any improvements of the goodness Q of the fits. In essence we are left with fits to the leading, likely effective, correction

$$F_{s;L} = F_s + \frac{a_1}{L}; \quad (17)$$

and, due to our small lattice sizes, finite-size corrections are so big that the best we can do is a fit of the interface tensions from the largest two lattices, $L = 12$ and 16 . This yields the estimates

$$F_s = 0.03002 \text{ (24) at } \beta = 0.232; \quad (18)$$

and

$$F_s = 0.30583 \text{ (68) at } \beta = 0.3; \quad (19)$$

which are (under the circumstances of our limited system sizes) in reasonably good agreement with results of Hasenbusch and Pinn (HP) [27], for a review see Ref. [28]. Again, our error bars are purely statistical and do not reflect systematic errors due to our small lattice sizes.

Our result (18) at $\beta = 0.232$ is lower than the multimagnetical estimate of Ref. [16]. This moves into the right direction and indicates that the resolution of the inconsistency between the multicanonical and the HP estimate at $\beta = 0.232$, discussed in the paper by Zinn and Fisher [29], has its origin in the complex finite-size scaling behavior of $F_{s;L}$ estimates from the magnetization, which could be resolved by simulating larger systems. It is notable that this difficulty of the extrapolation appears to be limited to a small neighborhood of $\beta = 0.232$, as the multimagnetical F_s estimates [16] at $\beta = 0.227$ and $\beta = 0.2439$ are perfectly consistent with HP, see Fig. 1 of Ref. [29].

IV. SUMMARY AND CONCLUSIONS

In Sect. II we have analyzed the critical behavior of the overlap variable q . In essence agreement with the standard scaling picture is found, but with some new insights. In particular, we exhibit in Table I that scaling

appears to be connected to a small q (but still large $q^0 = qL^{2/\nu}$) neighborhood. It may be worthwhile to check whether the magnetic probability distribution, for which comparable simulations are easier to perform, exhibits a similar behavior. Further, we find support in favor of standard large deviations (4), instead of the form (13) derived from Gumbel's first asymptote (3).

Below the critical point, in Sect. III, we estimate interface free energies from our overlap probability densities. The results are smoother than those from the probability density of the magnetization [16] and tend to reconcile discrepancies noted in Ref. [29]. But, like at the critical point, considerably larger lattices would be needed to reach high precision results.

ACKNOWLEDGMENTS

We would like to thank Gernot Münster and Uwe-Jens Wiese for helpful correspondence. This work was in part supported by the US Department of Energy under contract DE-FG 02-97ER 41022. The numerical simulations were performed on the Compaq SC 256 computer of CEA in Grenoble under grant p526 and on the T3E computer of NIC in Jülich under grant hm z091.

-
- [1] K. Binder and A.P. Young, Rev. Mod. Phys. 58, 801 (1986).
 - [2] M. Mezard, G. Parisi, and M.A. Virasoro, Spin Glass Theory and Beyond (World Scientific, Singapore, 1987).
 - [3] K.H. Fischer and J.A. Hertz, Spin Glasses (Cambridge University Press, Cambridge, 1991).
 - [4] A.P. Young (ed.), Spin Glasses and Random Fields (World Scientific, Singapore, 1997).
 - [5] M.E. Fisher, in Critical Phenomena, Proc. 1979 E. Fermi Int. School of Physics, Vol. 51, M.S. Green (ed.) (Academic Press, New York, 1971), p. 1.
 - [6] B.A. Berg and W. Janke, Phys. Rev. Lett. 80, 4771 (1998).
 - [7] S.T. Bramwell, K. Christensen, J.-Y. Fortin, P.C.W. Holdsworth, H.J. Jensen, S. Lise, J.M. Lopez, M. Nicodem, J.-F. Pinton, and M. Sellitto, Phys. Rev. Lett. 84, 3744 (2000).
 - [8] S.T. Bramwell, J.-Y. Fortin, P.C.W. Holdsworth, J.-F. Pinton, B. Portelli, and M. Sellitto, Phys. Rev. E 63, 041106 (2001).
 - [9] The exponent a takes the values $a = 1; 2; 3; \dots$, corresponding, respectively, to the distribution of the first, second, third, \dots smallest random number of a set of N random numbers, $N \rightarrow 1$. This result is due to Fisher and Tippett, Kawata and Smimov. Gumbel [10] wrote the first book on the subject and coined the name first asymptote for the $a = 1$ result.

- [10] E.J. Gumbel, *Statistics of Extremes* (Columbia University Press, New York, 1958).
- [11] J. Galambos, *The Asymptotic Theory of Extreme Order Statistics*, second edition (Krieger Publishing Co., Malabar, Florida, 1987).
- [12] L. Boltzmann, *Wiener Berichte* 276, 373 (1877).
- [13] B.A. Berg, U. Hansmann, and T. Neuhaus, *Phys. Rev. B* 47, 497 (1993).
- [14] B.A. Berg, A. Billoire, and W. Janke, *Phys. Rev. E* 65, 045102(R) (2002).
- [15] G.S. Pawley, R.H. Swendsen, D.J. Wallace, and K.G. Wilson, *Phys. Rev. B* 29, 4030 (1984).
- [16] B.A. Berg, U. Hansmann, and T. Neuhaus, *Z. Phys. B* 90, 229 (1993).
- [17] B.A. Berg, A. Billoire, and W. Janke, *Phys. Rev. B* 61, 12143 (2000).
- [18] K. Binder, *Z. Phys. B* 43, 1699 (1981).
- [19] E. Brezin and J. Zinn-Justin, *Nucl. Phys. B* 257, 867 (1985).
- [20] A. Pelissetto and E. Vicari, cond-mat/0012164, submitted to *Phys. Rep.*.
- [21] W.H. Press, S.A. Teukolsky, W.T. Vetterling, and B.P. Flannery, *Numerical Recipes in Fortran 77: The Art of Scientific Computing*, second corrected edition (Cambridge University Press, Cambridge, 1996).
- [22] M. Caselle, R. Fiore, F. Gliozzi, M. Hasenbusch, K. Pinn, and S. Vinti, *Nucl. Phys. B* 432, 590 (1994).
- [23] M.P. Gelfand and M.E. Fisher, *Physica A* 166, 1 (1990).
- [24] J.J. Morris, *J. Stat. Phys.* 69, 539 (1991).
- [25] A. Billoire, T. Neuhaus, and B.A. Berg, *Nucl. Phys. B* 413, 795 (1994).
- [26] P. Hoppe and G. Münster, *Phys. Lett. A* 238, 265 (1998).
- [27] M. Hasenbusch and K. Pinn, *Physica A* 203, 189 (1994).
- [28] M. Hasenbusch, *Int. J. Mod. Phys. C* 12, 911 (2001).
- [29] S.-Y. Zinn and M.E. Fisher, *Physica A* 226, 168 (1996).